2D Magnetic Resonance Electrical Property Tomography based on B_1^- field mapping

Yuqing Wan, Michiro Negishi, and R. Todd Constable

Abstract —**Magnetic Resonance Electrical Property Tomography (MREPT) is a method to visualize electrical conductivity and permittivity distributions in the object. Traditional MREPT relies on either the radio frequency (RF) transmit field (B_1^+) mapping, or using a transmit/receive RF coil, to compute tissue's electrical conductivity and permittivity. This paper introduces an alternative approach based on the reconstructed receive field (B_1^-). By solving a system of homogeneous equations consisting of the signal ratios from multi-channel receive coils, the receive field distribution with both magnitude and phase can be computed. Similar to B_1^+ based MREPT method, the conductivity and permittivity in the imaging object can be calculated from the B_1^- field. We demonstrated the feasibility to image electrical property contrasts through computer simulated studies and phantom experiments. Although this study focuses on the 2D reconstruction, the presented method can be extended to full 3D. This method can be applied to regular MR imaging collected with multi-channel receive coils, and therefore, tissue anomaly based on electrical properties can potentially be revealed with a higher imaging quality, providing useful information for clinical diagnosis.**

I. Introduction

Conventional magnetic resonance (MR) imaging provides useful anatomical and/or pathological information based on tissue's proton density and the relaxation time (T1 or T2). Electrical properties (i.e. conductivity and permittivity) were first introduced by Haacke et al. 1991 as another contrast mechanism to differentiate tissues using MR [1]. After Wen [2] and Katscher et al. [3] developed and implemented the Magnetic Resonance Electrical Property Tomography (MREPT) method, a number of studies have been reported focusing on both the theoretical framework [4-6] and its clinical applications [7, 8].

The MREPT method relies on the accurate mapping of the transmit field (B_1^+) of the radio frequency (RF) coils, because the field distribution is determined by the tissue's electrical properties and the field's magnitude is accessible with existing B_1^+ mapping techniques including the curve-fitting method [9], the double-angle method [10] and the Bloch-Siegert shift method [11]. However, the phase information of B_1^+ field is often difficult to obtain directly. As a result, a transmit/receive coil must be employed to utilize the conjugate-symmetric feature of the transmit and receive fields in order to compute the electrical properties [12, 13]. Alternatively, the transmit field phase can be analytically computed with the 'Local Maxwell Tomography' method, but it requires multiple, independent RF transmit sequences [5].

The receive field of the RF coils, B_1^-, can also be used to compute the electrical properties, similar to the B_1^+ field. The B_1^- is historically computed after obtaining the B_1^+ maps for phantoms with known or homogenous proton density. Recently another B_1^- estimation method was reported, but it requires optimization and elaborate electromagnetic field modeling [14].

This study introduces a novel approach to assessing tissue electrical properties based on the computed 2D B_1^- field from signal ratios of multiple receive channels. Conventional B_1^+ mapping is not necessary and both conductivity and permittivity can be calculated. Mathematical formulation is presented followed by computer simulation studies and phantom experiments to demonstrate the feasibility of the method.

II. Theory

The signal measured on the receive channels is a combination of transmit field $B_1^+(\boldsymbol{r})$, magnetization $M_0(\boldsymbol{r})$ including proton density and relaxation effects, and the coil's receive field $B_1^-(\boldsymbol{r})$, for a voxel located at $\boldsymbol{r}$, as shown in (1):

$$S(\boldsymbol{r}) = -2j\omega \cdot M_0(\boldsymbol{r}) \cdot \sin(\gamma\tau|B_1^+(\boldsymbol{r})|) \cdot \frac{B_1^+(\boldsymbol{r})}{|B_1^+(\boldsymbol{r})|} \cdot B_1^-(\boldsymbol{r})^* \quad (1)$$

where j is the imaginary quantity $\sqrt{-1}$, ω the angular resonance frequency, γ the gyromagnetic ratio, τ the duration of applied RF excitation and the asterisk denotes a complex conjugate. Note that $B_1^-(\boldsymbol{r})$ may not be associated with $B_1^+(\boldsymbol{r})$ since the transmit and receive coils may be separate coils.

The $B_1^-(\boldsymbol{r})$ field is equivalent to the magnetic field in the negatively rotating frame, generated by a unit

Y. Wan, M. Negishi and R. T. Constable are with Yale University, New Haven, CT 06511 USA (203-737-5995; fax: 203-785-6534; e-mail: yuqing.wan@yale.edu, michiro.negishi@yale.edu, todd.constable@yale.edu).

978-1-4244-7929-0/14/$26.00 ©2014 IEEE

amplitude, zero phase current flowing on a receive coil [15]:

$$B_1^-(r) = \frac{(B_{1x}(r) - jB_{1y}(r))^*}{2} \quad (2)$$

where $B_{1x}(\boldsymbol{r})$ and $B_{1y}(\boldsymbol{r})$ are the x- and y- components of the resulting magnetic field from the unit current.

The Maxwell wave equations of the magnetic field can be reduced to Helmholtz equations:

$$\nabla^2(B_1^-(\boldsymbol{r})^*) + k^2(B_1^-(\boldsymbol{r})^*) = 0 \quad (3)$$

with the assumption of local constant electrical properties k [2], where ∇^2 is the Laplace operator and $k = \sqrt{\omega^2\mu\varepsilon(1 + \frac{\sigma}{j\omega\varepsilon})}$ is the wave number, μ, ε and σ denoting permeability, permittivity and conductivity of the medium, respectively.

By taking the ratio of a single channel (m) signal to the signal sum of all L channels, the effects of proton density, relaxation and transmit field can be eliminated, leaving only the receive fields relations:

$$R_m(\boldsymbol{r}) = \frac{S_m(\boldsymbol{r})}{S_{sum}(\boldsymbol{r})} = \frac{B_{1m}^-(\boldsymbol{r})^*}{B_{1sum}^-(\boldsymbol{r})^*}, \quad m \in 1,2,\cdots,L \quad (4)$$

Combining (3) and (4) and approximating the Laplacian with second order center difference, we have the center equation for each voxel:

$$\begin{aligned}
&\frac{1}{\Delta x^2}\left(\frac{R_m(x+\Delta x,y,z)^*}{R_m(x,y,z)^*} - 1\right)B_{1sum}^-(x+\Delta x,y,z) \\
&+\frac{1}{\Delta x^2}\left(\frac{R_m(x-\Delta x,y,z)^*}{R_m(x,y,z)^*} - 1\right)B_{1sum}^-(x-\Delta x,y,z) \\
&+\frac{1}{\Delta y^2}\left(\frac{R_m(x,y+\Delta y,z)^*}{R_m(x,y,z)^*} - 1\right)B_{1sum}^-(x,y+\Delta y,z) \\
&+\frac{1}{\Delta y^2}\left(\frac{R_m(x,y-\Delta y,z)^*}{R_m(x,y,z)^*} - 1\right)B_{1sum}^-(x,y-\Delta y,z) \\
&+\frac{1}{\Delta z^2}\left(\frac{R_m(x,y,z+\Delta z)^*}{R_m(x,y,z)^*} - 1\right)B_{1sum}^-(x,y,z+\Delta z) \\
&+\frac{1}{\Delta z^2}\left(\frac{R_m(x,y,z-\Delta z)^*}{R_m(x,y,z)^*} - 1\right)B_{1sum}^-(x,y,z-\Delta z) = 0.
\end{aligned} \quad (5)$$

A system of homogeneous equations can be constructed with (5) for every voxel in the FOV. The solution of the receive field B_{1sum}^- at each voxel can be substituted into (3) and the electrical properties can be computed. In this study, due to the limited computational resources, the magnetic field variation along the z direction is neglected and only a 2D field distribution is considered (last two terms of (5) are omitted).

III. Methods

A. Simulation studies

An 8-channel receive coil was modeled in the simulation software Comsol 4.3a, AC/DC module (Comsol, Inc., Burlington, MA, USA). Each receive channel was simulated as a straight wire along the axial direction on the surface of a cylindrical coil, and therefore, the magnetic field could be approximated by a constant along the z direction. 2D magnetic field was simulated on the central cross section plane and the receive field was computed with (2). The ratios of the signals from (4) were imported in Matlab 2012b (Mathworks, Natick, MA, USA) to reconstruct B_{1sum}^- and compute ε and σ on a Linux platform (Centos 6.4) with 6 Intel Xeon CPUs (3.33 GHz) and a memory of 94.5 Gigabytes. The simulation configuration was demonstrated in Fig. 1, where the coil diameter was 12.5 cm, FOV 5×5 cm, a contrast inclusion (diameter 1.5 cm) located 1.2 cm off center on the x-axis, and the background $\varepsilon_r = 38$ and $\sigma = 0.2$ S/m. The inclusion was specified to have $\sigma_c = 0.4$ S/m and $\varepsilon_{r\_c} = 75$ in the conductivity and permittivity experiments, respectively.

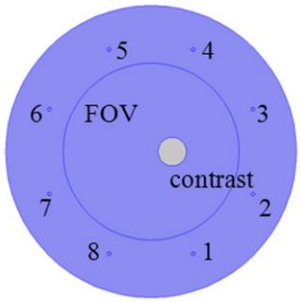

Figure 1. Cross section view of the simulation study configuration. Eight straight microstrip receive coil elements are numbered. The FOV is represented by the circle inside the 8 coil elements.

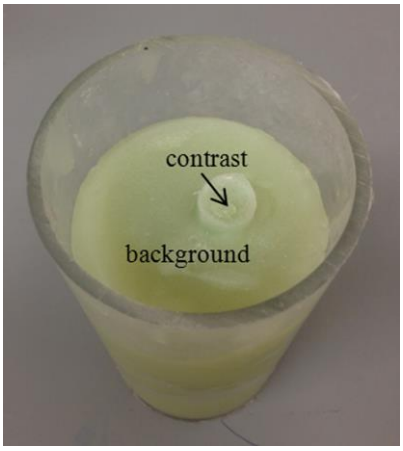

Figure 2. A photograph of the agar phantom depicting the relative size and location of the contrast inclusion and the background.

B. *Phantom experiments*

A cylindrical agar phantom (12 cm in diameter and 10 cm in length) was tested with a 3T MR scanner (Siemens TIM Trio, Erlangen, Germany). The weight ratio of agar (AB01185, American Bioanalytical, Inc, Natick, MA, US): NaCl:$CuSO_4$:deionized water was 4:1:0.06:100 in the background, and the contrast inclusion contained 2% NaCl for an elevated conductivity. The cylindrical inclusion was positioned approximately 1 cm off center, with a diameter of 2 cm (Fig. 2). The custom made receive coil used in the experiment featured 8 microstrip elements aligned axially on the surface of a 12.5 cm diameter, 12 cm long cylinder. The MR images were collected with a gradient echo (TR = 1000 ms, TE = 5 ms and 90^0 flip angle) transmitted from the body coil, 8 averages (NEX), 300×300 mm FOV, 1.2×1.2×10 mm voxel size and an image matrix of 256×256. The signal sum $S_{sum}(\boldsymbol{r})$ was computed by adding complex signals from individual coil elements after phase corrections for a circular polarized magnetic field. Image data for 9 axial slices were acquired and the central slice was used to compute the B_{1sum}^- field and electrical properties.

IV. Results

The reconstructed conductivity and permittivity images for the simulation studies are shown in Fig. 3. The average reconstructed conductivity and permittivity in the inclusion regions were 2.24 S/m and 43.77 respectively, compared to 0.28 S/m and 21.30 in the background. The reconstructed phantom conductivity image is shown in Fig. 4, with an average conductivity of 9.5 S/m in the inclusion and 1.93 S/m in the background.

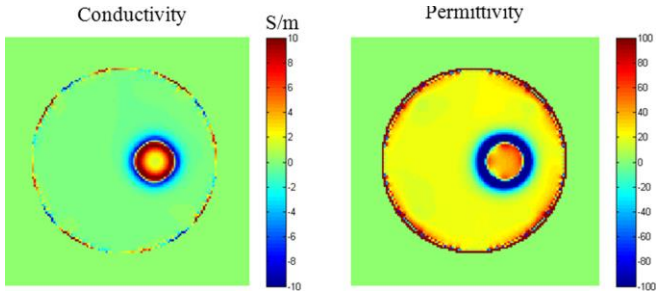

Figure 3. Reconstructed conductivity and permittivity images for the simulation study.

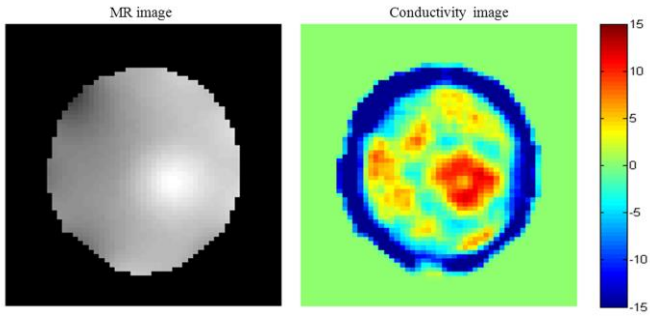

Figure 4. Left: Acquired MR magnitude for the phantom experiment. Right: Reconstructed conductivity image from the same data.

V. Discussion

In order to reconstruct the B_1^- field, a system of ill-conditioned homogeneous equations (5) needs to be solved. However, the solution is inherently not unique: a zero vector satisfies the equation and is a trivial solution; an existing solution multiplied by any non-zero constant is also a solution. Therefore, the absolute B_1^- is mathematically impossible to compute; instead, the ratio of the receive field among voxels is reconstructed.

If we reorganize the equations in the matrix form:

$$\underline{\underline{A}} \cdot \underline{B_{1sum}^-} = 0 \tag{6}$$

where $\underline{\underline{A}}$ is a matrix consisting of coefficients and $\underline{B_{1sum}^-}$ is a vector of unknown receive field at individual voxels, the nonzero solution $\underline{B_{1sum}^-}$ resides in the null space of $\underline{\underline{A}}$. Generally, the singular value decomposition (SVD) method can be used to compute the null space [16], however, the finite difference approximation for the Laplacian and inevitable measurement noise make it impossible to find the true null space. As a result, the direct solution is not representative of the true receive field (verified with simulation studies, not shown here).

Instead, we used a different approach to solve for B_1^-. Additional constraints were imposed to convert the equations to inhomogeneous ones under the assumption that the sum of the receive field equals unity. This constraint ensures that the least squares solutions can be achieved with the pseudo-inverse method. Additionally, we imposed regularization for continuous B_1^- distribution in the neighboring voxels to reduce inter-voxel field variations induced by measurement noise. Consequently, although the solution may not be the exact B_1^- field, the contrast information of electrical properties was well preserved. As equation (3) indicates, only the contrast of the receive magnetic field is relevant for the computation of the conductivity and permittivity distributions.

The flip angle was selected 90^0 in the phantom experiment to ensure largest magnetization in the transverse plane to achieve highest signal measurements. The phantom experiment used 8 averages in order for high SNR, but practically, this number can be reduced when the sample is close to the receive array to decrease the scan time.

Image artifacts at the electrical property contrast interfaces resulted from the assumption that the local wavenumber k is constant. Similar artifacts were also observed in other studies and a method for reconstruction in separate compartments could be applied to mitigate this issue [17]. Besides the non-constant local k artifacts, some

fluctuations in the background region were also observed in the reconstructed conductivity image, which may result from small variations of the receive field in the z-direction (microstrip coil elements were not infinitely long), measurement noises and possibly inhomogeneity in the agar phantom's composition. Total variation regularization may be used to mitigate the fluctuation. Additionally, *a priori* anatomic information from MR images may also be incorporated to improve electrical property reconstruction.

The described method is not limited to 2D electrical property reconstruction. It can be extended to a full 3D reconstruction as shown in (5) with any receive array configuration. For a FOV of $X \times Y \times Z$ voxels, a system of $(X-2)(Y-2)(Z-2)(L-1)$ equations will be constructed with $(XYZ-8)$ unkowns (the field at 8 corners of the FOV cannot be computed). 3D reconstruction will add Laplacian term in the z direction, potentially providing more inter-voxel information in the system of equations. However, this exceeds our current computational power for typical MR images, but we are exploring ways to efficiently utilize computer memories and ultimately implement the full 3D computation. For example, the 3D FOV may be reduced into blocks and each block can be solved independently. The boundary voxels will be constrained to ensure the field continuity across blocks. Additionally, we will explore optimal receive array configurations and B_1^- field patterns to facilitate the computation and improve electrical property reconstruction.

VI. Conclusion

This study presented a method of measuring the electrical properties of tissues in MRI using multiple MR receive coils based on the reconstructed B_1^- field. Simulation studies and phantom experiments demonstrated the feasibility of the method to image conductivity and permittivity contrasts. This method can be potentially applied to regular multi-channel receive coils to reveal tissue anomalies based on electrical properties and may provide useful information for clinical diagnosis.

References

[1] Haacke, E.M., et al., Extraction of Conductivity and Permittivity Using Magnetic Resonance Imaging. Physics in Medicine and Biology, 1991. 36(6): p. 723-734.

[2] Wen, H., Non-invasive quantitative mapping of conductivity and dielectric distributions using the RF wave propagation effects in high field MRI. Medical Imaging 2003: Physics of Medical Imaging, Pts 1 and 2, 2003. 5030: p. 471-477.

[3] Katscher, U., et al., Determination of electric conductivity and local SAR via B1 mapping. IEEE Transaction on Medical Imaging, 2009. 28(9): p. 1365-74.

[4] Bulumulla, S.B., S.K. Lee, and D.T. Yeo, Conductivity and permittivity imaging at 3.0T. Concepts in Magnetic Resonance, 2012. 41B(1): p. 13-21.

[5] Sodickson, D.K., et al. Local Maxwell tomography using transmit-receive coil arrays for contact-free mapping of tissue electrical properties and determination of absolute RF phase. in Proceedings of the 20th Scientific Meeting of the International Society of Magnetic Resonance in Medicine (ISMRM'12). 2012. Melbourne, Australia.

[6] Liu, J., et al., Determining electrical properties based on B(1) fields measured in an MR scanner using a multi-channel transmit/receive coil: a general approach. Physics in Medicine Biology, 2013. 58(13): p. 4395-408.

[7] Katscher, U., et al. Estimation of breast tumor conductivity using parabolic phase fitting. in Proceedings of the 20th Scientific Meeting of the International Society of Magnetic Resonance in Medicine(ISMRM'12). 2012. Melbourne, Australia.

[8] Voigt, T., U. Katscher, and O. Doessel, Quantitative Conductivity and Permittivity Imaging of the Human Brain Using Electric Properties Tomography. Magnetic Resonance in Medicine, 2011. 66(2): p. 456-466.

[9] Maier, J.K. and G.H. Glover, Method for mapping the RF transmit and receive field in an NMR system, in Google Patents. 1991.

[10] Wang, J., et al., Measurement and correction of transmitter and receiver induced nonuniformities in vivo. Magnetic Resonance in Medicine, 2005. 53(2): p. 408-17.

[11] Sacolick, L.I., et al., B1 mapping by Bloch-Siegert shift. Magnetic Resonance in Medicine, 2010. 63(5): p. 1315-22.

[12] van Lier, A.L., et al., B1(+) phase mapping at 7 T and its application for in vivo electrical conductivity mapping. Magnetic Resonance in Medicine, 2012. 67(2): p. 552-61.

[13] Zhang, X., et al., Complex B1 mapping and electrical properties imaging of the human brain using a 16-channel transceiver coil at 7T. Magnetic Resonance in Medicine, 2013. 69(5): p. 1285-96.

[14] Jin, J., et al., Inverse field-based approach for simultaneous B-1 mapping at high fields - A phantom based study. Journal of Magnetic Resonance, 2012. 217: p. 27-35.

[15] Hoult, D.I., The principle of reciprocity in signal strength calculations - A mathematical guide. Concepts in Magnetic Resonance, 2000. 12(4): p. 173-187.

[16] Bretscher O. Linear algebra with applications. Upper Saddle River, NJ: Prentice Hall; 2001. xv, 478 p. p.

[17] Katscher, U., D.H. Kim, and J.K. Seo, Recent progress and future challenges in MR electric properties tomography. Computational and Mathematical Methods in Medicine, 2013. 2013: p. 546562.W.-K. Chen, *Linear Networks and Systems* (Book style). Belmont, CA: Wadsworth, 1993, pp. 123–135.